Acta Neuropathologica Communications

RESEARCH

Open Access

LXR agonist rescues synaptic dysfunction and degeneration in SPG3A patient-specific iPSC-derived neurons

Gitika Thakur[1], Rutuja Dhanukate[1], Yongchao Mou[1,2], Priya Kunhiraman[1], Archana Khadilkar[1], Siddharth Srivastava[3], Julian E. Alecu[3], Darius Ebrahimi-Fakhari[3], Zhenyu Chen[1,2], Craig Blackstone[4,5*] and Xue-Jun Li[1,2*]

Abstract

Hereditary spastic paraplegias (HSPs) comprise a large, heterogeneous group of inherited disorders characterized by length-dependent axonal degeneration of corticospinal motor neurons, leading to lower extremity spasticity and gait impairment. Currently, there are no effective treatments for HSPs targeting axonal dysfunction. Our previous study showed that lipid defects in glial cells result in degeneration of iPSC-derived cortical projection neurons (PNs) in SPG3A, the most common early-onset form of HSP caused by autosomal dominant mutations in the *ATL1* gene encoding atlastin-1. However, how cortical PNs degenerate and whether therapeutic compounds targeting lipid defects can effectively mitigate degeneration in human *ATL1* neurons remain unclear. Here, by comparing SPG3A patient iPSC-derived neurons with control cells using RNA-sequencing, we identified synaptic dysfunction as a top-altered pathway in addition to lipid-related pathways. To examine the novel role of synaptic dysfunction in SPG3A, we generated patient-specific iPSCs from two SPG3A patients with distinct missense mutations and differentiated them into cortical PNs. We observed significant reductions of synaptic genes and proteins in cortical PNs from both SPG3A-P342S and SPG3A-M408T patient iPSCs, emphasizing synaptic dysfunction in SPG3A neurons. Calcium imaging revealed a significant reduction of activity in SPG3A cortical neurons compared to control neurons, further supporting functional deficits in SPG3A neurons. To further examine the role of these processes in HSP pathogenesis, we treated cells with LXR623, an orally bioavailable liver-X-receptor (LXR) agonist that can modulate lipid metabolism and transfer. LXR623 significantly mitigated the reduction in synaptic proteins and calcium activity and rescued axonal degeneration and apoptosis in SPG3A cortical PNs. Furthermore, analyses of lipid and synaptic genes and proteins revealed that LXR623 treatment effectively restored mRNA expression patterns for these pathways in SPG3A neurons. Taken together, our data demonstrate the role of synaptic dysfunction in degeneration of SPG3A neurons and highlight the therapeutic potential of an LXR agonist in mitigating human cortical neuron degeneration in HSP.

Keywords Hereditary spastic paraplegias, iPSC, Axon degeneration, Lipid homeostasis, Synaptic dysfunction

*Correspondence:
Craig Blackstone
cblackstone@mgh.harvard.edu
Xue-Jun Li
xjli23@uic.edu
[1]Department of Biomedical Sciences, University of Illinois College of Medicine Rockford, Rockford, IL 61107, USA
[2]Department of Biomedical Engineering, University of Illinois Chicago, Chicago, IL 60607, USA
[3]Department of Neurology, Boston Children's Hospital, Harvard Medical School, Boston, MA 02115, USA
[4]Movement Disorders Division, Department of Neurology, Massachusetts General Hospital and Harvard Medical School, Boston, MA 02114, USA
[5]MassGeneral Institute for Neurodegenerative Disease, Massachusetts General Hospital, Charlestown, MA 02129, USA

Introduction

Hereditary spastic paraplegias (HSPs) are a large, heterogeneous group of inherited neurological disorders characterized by length-dependent degeneration of corticospinal motor neuron axons, leading to spasticity of the lower limbs and gait impairment [7, 16, 42]. A genetically diverse condition, HSP can result from mutations of more than 90 distinct genes [6, 17, 19, 33]. SPG3A, the most common early-onset form of HSP, results from autosomal dominant, mostly missense mutations in the *ATL1* gene that encodes the atlastin-1 protein [28, 30, 57]. The organization of the tubular endoplasmic reticulum (ER) in cells is maintained by atlastin-1 [40, 56], and atlastin-1 can regulate the size of lipid droplets both in intestinal cells of zebrafish and in Drosophila fat bodies [24]. This is related to atlastin's role on ER membranes, since ER is critical for lipid metabolism and trafficking. Lipids are essential components of neuronal membranes and have a variety of effects on brain function [9, 38]. Alterations in ER morphology have been implicated in multiple distinct types of HSPs [34, 40], though detailed mechanisms by which ER defects lead to dysfunction and degeneration of cortical PNs remain largely unclear.

Along with cortical PNs, non-neuronal glial cells are also impacted by *ATL1* mutation [29]. Glia are essential for development of neurons, their migration to final sites of residence, formation of synapses, regulation of synaptic activity, and regulation of ion concentrations along synapses [21]. They provide scaffolding for neuronal migration and mediate axonal growth and synaptic development. The synaptic membrane contains high concentrations of cholesterol and unsaturated fatty acids, which are crucial factors in specifying various biological processes. These processes include membrane fluidity, vesicle formation and fusion, ion channel function, and the creation of specialized microdomains that aid in intercellular communication [3, 38]. Cholesterol plays a significant role in lipid rafts and is thought to be necessary both postsynaptically for the stability and clustering of neurotransmitter receptors and presynaptically for the production of synaptic vesicles [48]. The ability of neurons to synthesize lipids including cholesterol is significantly reduced after birth, and neurons acquire lipids generated by astrocytes to maintain the creation and function of synapses [32, 37]. The transfer of lipids to neurons is mediated by apolipoprotein E (ApoE)-containing lipoproteins, which are crucial for the development, maturation, and maintenance of synapses in vitro [12, 18, 36]. Previously, studies have reported reduced ApoE and lipid deficiency in HSP. However, whether lipid defects lead to synaptic dysfunctions and how axons degenerate in patients await further investigation.

Currently, there are no effective treatments to directly mitigate nerve degeneration for HSP. The development of stem cell technology, especially the generation of patient-specific induced pluripotent stem cells (iPSCs) [13, 20, 47, 51], offers unique resources to generate different neural subtypes to study neurological diseases [15, 41, 45, 53]. By reprogramming fibroblast cells of a SPG3A patient with a heterozygous, pathogenic missense variant in *ATL1* (NM_015915.5: c.1024C > T, p.P342S), we generated patient iPSCs and differentiated these iPSCs into cortical PNs, showing disease-specific axonal defects [55]. We further identified impaired lipid metabolism and trafficking in SPG3A iPSC-derived neural cells [29], although how lipid deficiency leads to the dysfunction and degeneration of SPG3A neurons and whether targeting lipid defects can effectively mitigate neuronal degeneration remain unclear. In the current study, we identified synaptic dysfunction as a major pathological change in SPG3A from unbiased genomics analyses of patient iPSC-derived neural cells. We then established iPSCs from another SPG3A patient with a distinct *ATL1* mutation (NM_015915.5: c.1223T > C, p.M408T) and severe clinical presentation [2] and identified aberrant synaptogenesis in neurons with both mutations (p.P342S and p.M408T). To further examine the role of synaptic dysfunction and the interplay between lipid and synaptic deficits in SPG3A, we tested the effects of a lipid-targeting compound, LXR623 which is an orally bioavailable LXR agonist that can cross the blood brain barrier, providing a therapeutic candidate for SPG3A.

Materials and methods

SPG3A patient fibroblast cells and the reprogramming of fibroblast cells into iPSCs

Skin punch biopsies were obtained following a clinical research procedure (protocols #IRB-P00016199, #IRB-P00033016) authorized by the Institutional Review Board at Boston Children's Hospital. Dermal fibroblasts from a patient with SPG3A (p.M408T) were obtained and cultured according to conventional protocols, which were then used to generate iPSCs. The Institutional Biosafety Committee of the University of Illinois approved all iPSC research.

The Sendai virus method was used to generate iPSC lines from human dermal fibroblasts using the CytoTune® 2.0 Sendai reprogramming Kit from Invitrogen (USA). Fibroblasts with a passage number less than 5 were plated onto a 6-well plate in fibroblast medium so that they were 50–80% confluent on the day of transduction (Day 0) using CytoTune® 2.0 Sendai reprogramming vectors followed by overnight incubation. The next day (Day 1), the medium was replaced with fresh complete fibroblast medium to remove the reprogramming vectors. Spent medium was replaced every other day until Day 6. After 1 week, transduced cells were plated on mouse embryonic fibroblasts (MEFs) and then switched to iPSC medium.

Until Day 28, spent medium was replaced every day, and culture vessels were monitored for the emergence of iPSC colonies. After 3 weeks, iPSC colonies were ready for transfer, and undifferentiated iPSCs were picked and plated onto fresh MEF culture dishes for expansion. To further evaluate pluripotency, teratoma assays were conducted to assess the capacity of iPSCs to differentiate into all three embryonic germ layers in vivo [31, 52]. Briefly, SCID-beige mice at about 6 weeks of age were injected one time subcutaneously (s.c.) with 0.10 ml stem cell suspension (about 1 million cells). After injection, mice were monitored regularly for tumor formation. At about 8 weeks after injection, mice were euthanized using CO_2 and the tumors were dissected, followed by fixation and HE (hematoxylin and eosin) staining. The Institutional Biological Research Committee at the University of Illinois (IACU protocol # 1892409) approved the teratoma assay.

iPSC authentication and sendai virus clearance assessment

The iPSC cell lines were authenticated by Short Tandem Repeats (STR) testing at the Sequencing Core at Northwestern University. Donor fibroblast cell lines served as identity controls and STR profiles of the generated iPSCs were compared to these cell lines. Genomic DNA of both iPSC lines and donor fibroblast cell lines was extracted using a column-based extraction kit. Purified DNA samples were prepared and sent to the Sequencing Core at Northwestern University for STR genotyping analysis. To assess Sendai virus clearance in iPSCs, Sendai viral vectors were detected by primers that specifically target Sendai virus. Genomic DNA was isolated from iPSCs and positive controls (fibroblast cells with viral infection) and used as a template for genomic DNA polymerase chain reaction (PCR). The presence of Sendai viral sequences was measured by PCR using primers for *SeV, KOS, Klf4*, and *c-Myc* per the manufacturer's instructions (CytoTune-iPS 2.0 Sendai Reprogramming Kit guide, Invitrogen). Primer sequences are listed in Supplemental Table 1.

To further examine the role of *ATL1* mutations, we corrected the ATL1-P342S mutation using CRISPR-Cas9-mediated gene editing. The sequencing gRNA used to target *ATL1* was GCCCTTTTCAGTTACCCGC. The corrected line was generated in the Waisman iPSC core as previously reported [29]. The corrected iPSC clones were expanded and sent for Sanger sequencing to confirm the correction of the *ATL1* mutations. To further validate the corrected isogenic line, we examined the expression of pluripotency proteins in these corrected isogenic stem cells and performed karyotype analysis to confirm normal chromosomal organization.

Human iPSCs differentiation into cortical projection neurons

Human iPSCs used in the study include SPG3A patient-derived iPSCs (labeling as Patient 1 = ATL1-P342S, Patient 2 = ATL1-M408T) and wild-type control (labeling as Control or WT). P342S iPSC and WT control cells were generated previously [55]. All hPSCs were maintained on irradiated MEF (irMEF) feeder layers in 10 ng/ml FGF-2 (PeproTech)-supplemented hESC medium containing DMEM/F12 (Gibco), 1 × non-essential amino acids (NEAA, Gibco), 20% Knockout Serum Replacement (Gibco), 0.5 × GlutaMax (Gibco), and 0.1 mM β-mercaptoethanol (Sigma-Aldrich).

As previously documented [8, 10, 27], cortical PNs were generated by differentiation of iPSCs. Briefly, the human iPSCs were detached and grown in suspension for 4 days in hESC media without FGF-2 to produce embryonic bodies (EBs). 1 × N2 (Gemini Bio-Products), 2 μg/ml heparin (Sigma-Aldrich), and 1 × NEAA were added to DMEM/F12 medium to create neural induction medium (NIM). For the Day 4 EB culture, NIM media supplemented with 2 μM SB431532 (Stemgent) and 2 μM DMH1 (Selleckchem) was utilized. Stem cell aggregates (EBs) were attached to 6-well culture plates and cultured in NIM to stimulate the differentiation into neuroepithelial (NE) cells. Up to Day 17, the medium was changed every other day. NE cells were then detached and suspended in NIM with 1 × B27 (Gemini Bio-Products), 1 μM cAMP (Sigma-Aldrich), and 10 ng/ml IGF-1 (Pepro-Tech) to form neurospheres. Following Day 42, the neurospheres were plated onto coverslips coated with Matrigel (Gibco) and poly-L-ornithine (Sigma-Aldrich). After attaching the neurospheres to coverslips, half of the neural differentiation medium (NDM) was changed every other day to produce cortical PNs in regular neural cultures. Included in the NDM of standard brain cultures were 1 × N2, 1 × B27, 1 μM cAMP, 10 ng/ml IGF-1, 10 ng/ml hBDNF (PeproTech), and 10 ng/ml hGDNF (PeproTech).

Immunocytochemistry

After washing neural cultures on coverslips in ice-cold PBS, they were incubated for 20 min in ice-cold 4% paraformaldehyde (Sigma-Aldrich) in PBS. After washing with PBS, cell cultures were incubated with 0.2% Triton X-100 (Sigma-Aldrich) solution for 10 min to permeabilize the cells, followed by several washes with PBS. Samples were blocked with 10% donkey serum in PBS for 1 h and then incubated with primary antibodies diluted in the blocking solution (5% donkey serum and 0.1% Triton X-100 in PBS) overnight at 4 °C. Samples were then washed and incubated with secondary antibodies conjugated with fluorescence for visualization. Coverslips were rinsed with PBS, incubated with Hoechst to label nuclei,

and then mounted using Fluoromount-G (Southern Biotech). Primary antibodies used in this study were: anti-SOX2 (goat IgG, R&D Systems, 1:500); anti-NANOG (goat IgG, R&D Systems, 1:500); anti-SSEA4 (mouse IgG3, DSHB, 1:100); anti-OCT4 (mouse IgG, Santa Cruz, 1:200); anti- Ctip2 (rat IgG, Abcam, 1:2000), anti-Tau (rabbit IgG, Sigma, 1:200), and anti-synapsin (mouse IgG, Calbiochem, 1:100). For immunostaining of LXR623 treated neural cultures, 1 μM of LXR623 or DMSO was used for 7 days for measuring synapsin and axonal swellings (Tau staining) in neuronal cultures. At least three coverslips for each group were used for immunostaining, and a minimum of 5 fields on each coverslip were imaged using an Olympus confocal microscope or an Olympus IX83 microscope.

mRNA sequencing analysis

We performed mRNA-Seq experiments on cortical PN cultures derived from WT control and ATL1-P342S iPSCs. Week 10 control and *ATL1*-mutated cortical PN cultures were collected, and subjected to RNA isolation using TRIzol reagent (Invitrogen) following the manufacturer's instructions. Libraries were prepared using Illumina's specifications for polyA-plus stranded reactions. Samples were analyzed using an Illumina HiSeq4000 sequencer. Reads were mapped to the human hg19 genome. Metascape software was used for gene ontology analysis [54]. All genes in the genome were used as the enrichment background. Terms with a p-value < 0.01, a minimum count of 3, and an enrichment factor > 1.5 (the enrichment factor is the ratio between the observed counts and the counts expected by chance) were collected and grouped into clusters based on their membership similarities. Kappa scores were used as the similarity metric when performing hierarchical clustering on the enriched terms, and sub-trees with a similarity of > 0.3 were considered a cluster. The most statistically significant term within a cluster was chosen to represent the cluster. To further capture the relationships between the terms, a subset of enriched terms were selected and rendered as a network plot, where terms with a similarity > 0.3 are connected by edges. We selected the terms with the best p-values from each of the 20 clusters, with the constraint that there were no more than 15 terms per cluster and no more than 250 terms in total. The network was visualized using Cytoscape, where each node represents an enriched term and is colored first by its cluster ID.

Axonal swelling analysis

Cortical neuron cultures were labeled with the axonal marker Tau in long-term cultured neurons to examine axonal swellings. A diameter more than twice that of the neighboring axon is considered an axonal swelling [11, 29]. Using ImageJ software, as previously described, the swelling density in the chosen region was computed by the swollen number over axon length. Each of the three separate coverslips in each group had at least five randomly chosen locations per coverslip that were examined.

Caspase 3/7 activity assay

Caspase 3 and 7 activities were measured using the Caspase-Glo 3/7 Assay kit (Promega) in accordance with the manufacturer's instructions. These activities are strongly correlated with the levels of apoptosis in cells. In short, neurons were dissociated into single cell suspension using Accutase. Following the manufacturer's procedure (Promega), cells were seeded into 96-well plates at a density of 5000 cells/well in 50 μl, lysed, and then treated with illuminance substrate by adding 50 μl of caspase-3/7 reagents. Using a Gen5 microplate reader (BioTek), the luminescence from each well was measured after 60 min of incubation at 37°C.

Calcium imaging

ATL1-mutated (ATL-P342S) and isogenic control iPSC lines were differentiated into cortical projection neurons using the protocol described above. To evaluate synaptic function, calcium imaging was performed on both patient and isogenic control neurons. Specifically, cells were loaded with the calcium-sensitive X-Rhod-1, AM, cell permeant dye (Invitrogen). A working solution containing 5 μM X-Rhod-1 is prepared immediately before use, and cells were incubated with this solution in an incubator for 1 h. After incubation, cells were washed twice with artificial cerebrospinal fluid (ACSF), allowed to normalize for 30 min, and then subjected to live-cell imaging using a Keyence microscope. Cells were stimulated by the application of 50 μM glutamic acid, and calcium levels were measured before (which reflects the basic activities) and after the addition of 50 μM glutamic acid. To investigate the impact of LXR623 on synaptic activity, patient-derived neurons were treated with LXR623 or vehicle control (DMSO) for 1 week, followed by calcium imaging. Multiple cellular regions were analyzed across at least three independent coverslips for each group using ImageJ software.

Cholesterol efflux measurement

SPG3A (ATL1-P342S) and isogenic control iPSC lines were differentiated into astrocytes as previously described [25, 29]. Briefly, the differentiation protocol for astroglial cells was the same as that used for cortical PNs until Day 21, when cortical neurospheres were cultured and expanded in NIM with 10 ng/ml hEGF and FGF2, with medium changes every 2–3 days. After 6 months of differentiation, cortical-glial spheres were dissociated

using Accutase, plated on laminin-coated 12-well Costar plates, and cultured in NIM supplemented with 10 ng/ml CNTF (PeproTech). After culturing cells for a week, cholesterol efflux measurements from both patient and isogenic control astrocyte cultures were conducted using the Cholesterol Efflux Assay Kit (Cell-based) (ab196985, Abcam). To evaluate cholesterol efflux, samples underwent the following treatment: SPG3A and control astrocyte cultures were subjected to 5 μM LXR623 or DMSO (vehicle) for three days.

The cholesterol efflux assessment was performed using the manufacturer's guidelines. Briefly, cells were labeled using a combination of 50 μl DMEM/F12 media and 50 μl Labeling Reagent per well, incubated for one hour at 37 °C in a CO_2 incubator. After labeling, the cells were allowed to incubate with 100 μl of Equilibration medium per well for 14 h under the same conditions. Upon completion of the incubation, the supernatant (medium) from each well was transferred to a 96-well plate. To solubilize adherent cells, 100 μl of lysis buffer was added, and the mixture was incubated for 30 min on an orbital shaker at room temperature. The lysate was then placed in a 96-well plate. Fluorescence of both the medium and lysates was quantified at Ex/Em = 485/523 nm using a BioTek FLX800 microplate reader. The calculation for cholesterol efflux used the formula: cholesterol efflux = fluorescence intensity of the medium / (fluorescence intensity of the cell lysate + medium), with each group analyzed in triplicate.

Western blotting

Cell pellets were collected and resuspended in lysis buffer with protease and phosphatase inhibitor cocktail (Protease inhibitor, PMSF, Phosphatase inhibitor reagent A and B) and lysed overnight. The cell debris was removed by centrifugation at 12,000 × g for 10 min at 4°C. Protein concentrations were determined using the Pierce™ BCA Protein Assay Kit (Thermo Scientific). Twenty μg of protein extracts was diluted in Laemmli buffer (Sigma-Aldrich) and heated at 70 °C for 15 min, then resolved by 10% SDS-PAGE at 80–110 V for 120 min (or until dye front reached the bottom), allowing size-based protein separation. A molecular weight marker precision plus protein dual color standards was included for size determination (BioRad). Following SDS-PAGE, separated proteins were transferred to a nitrocellulose membrane using a wet transfer system (45 V for 2.5 h or 200–400 mA for a similar time). The membrane was then blocked with 5% BSA in TBST (Tris-buffered saline Tween-20 buffer) for 1 h. Both blocking and antibody incubations were carried out in TBST containing 5% BSA. Primary antibodies used were mouse monoclonal anti β-actin antibody (Sigma-Aldrich, 1:1000) and rabbit monoclonal anti-synapsin antibody (Cell Signaling Technology, 1:1000). Horseradish peroxidase-conjugated secondary antibodies were detected with SuperSignal™ West Pico PLUS Chemiluminescent Substrate (Thermo Fisher Scientific). The quantification of Western blotting was performed using ImageJ and normalized against β-actin as a loading control.

Synapsin ELISA

Control and SPG3A neurons were treated with DMSO (vehicle control) or 1 μM LXR623 for 1 week. After treatment, cells were lysed with RIPA buffer, and the protein concentrations were measured using the BCA protein assay kit. The Synapsin-1 level in the lysates was determined by the Human Synapsin-1 ELISA Kit (EK713826, AFG Scientific) according to the manufacturer's recommendations. Briefly, cell lysates and Synapsin-1 standards were added to pre-coated wells of a microplate, incubated for 90 min at 37 °C, washed four times with wash solution, and incubated with HRP-conjugate reagent for 60 min at 37°C. Following another wash, the wells were incubated with 50 μl of Chromogen Solutions A and B for 15 min at 37 °C in the dark, and the reaction was stopped with Stop Solution. The absorbance was measured at 450 nm producing a standard curve, and the concentration of synapsin-1 in the cell lysate samples was calculated by interpolation and the concentration was normalized by protein concentration.

Real-time quantitative PCR

Using TRIzol (Invitrogen), total RNA samples were extracted from cortical neuronal cells. The High-Capacity cDNA Reverse Transcription Kit (Applied Biosystems) was utilized to produce cDNA from 1 μg of RNA. The PowerUp SYBR Green Master Mix (Applied Biosystems) was used in the QuantStudio 6 Flex Real-Time PCR System (Applied Biosystems) for real-time PCR. The settings for the PCR cycling were 50 °C for two min, 95 °C for three min, 45 two-step cycles at 95 °C for 15 s and 60 °C for 60 s, and a melt-curve stage at 95 °C for 15 s, 60 °C for 60 s, and 95 °C for 15 s. qRT-PCR primers are described in Supplemental Table 1. Cortical neural cultures were treated with LXR agonist or DMSO (control) for 1 week to ascertain the effects of the LXR agonist on gene expression related to cholesterol metabolism in wild-type control and patient specific iPSC-derived neural cultures.

Statistical analysis

All data are presented as mean ± SD. Statistical parameters including statistical value, statistical significance (p value), SD are detailed in the figures and figure legends. For statistical significance in mean values between two groups, we performed Student's t test. The statistical significance of mean values among multiple sample groups

was analyzed using ANOVA. $p < 0.05$ was considered significant.

Results

mRNA sequencing of patient specific cortical neural cells identified synaptic dysfunction in SPG3A

We previously generated iPSCs from a SPG3A patient (ATL1-P342S) and identified axonal degeneration and lipid defects [29, 55]. While the previous study established the link between lipid defects and neuron degeneration, how cortical PNs degenerate in SPG3A and whether therapeutic compounds targeting these lipid defects can effectively mitigate the impairment of human SPG3A neurons has remained unclear. The current study investigates the molecular underpinnings of neurodegeneration, utilizing unbiased mRNA sequencing analysis of SPG3A patient-derived iPSC-generated neural cells compared to healthy controls. About 8- to 10-week-old neural cells were selected because neural cells at this stage in culture SPG3A PNs start to show degeneration as indicated by impaired axonal transport; astrocytes are present at this stage (about 15%), and aberrant lipid transfer and trafficking are also observed in these cultures [29]. Our goal was to identify the molecular pathways underlying the degeneration of cortical neural cells by detailed analysis of their gene expression patterns.

We first identified all statistically enriched terms (based on the default choices under Express Analysis). Accumulative hypergeometric p-values and enrichment factors were calculated and used for filtering. Differentially expressed genes in patients as compared to the control were described by the heatmap (Fig. 1a), the color bar represents a downregulated (blue) or upregulated (red) mRNA. Analysis of mRNA expression in SPG3A cortical PN cultures pinpointed dysregulation of 20 top critical neurodevelopment-related pathways, prominently featuring impaired synaptic transmission, disrupted synaptic signalling, and compromised synapse structure (Fig. 1b). In agreement with our previous study [29], a significant reduction of lipid metabolism and lipid transfer pathways were observed in SPG3A cortical cells (Supplemental Table 2). We also observed changes in pathways critical for neuronal function including cell projections, neuronal system and brain development. Thus, the pathway analysis identified top altered pathways in SPG3A which are related to synapse structure and synaptic signalling.

Next, we performed network cluster analysis to identify the interactions between the clusters. The significantly altered terms were hierarchically clustered into a tree based on kappa-statistical similarities among their gene memberships (like what is used in the NCI DAVID site). Then, a 0.3 kappa score was applied as the threshold to

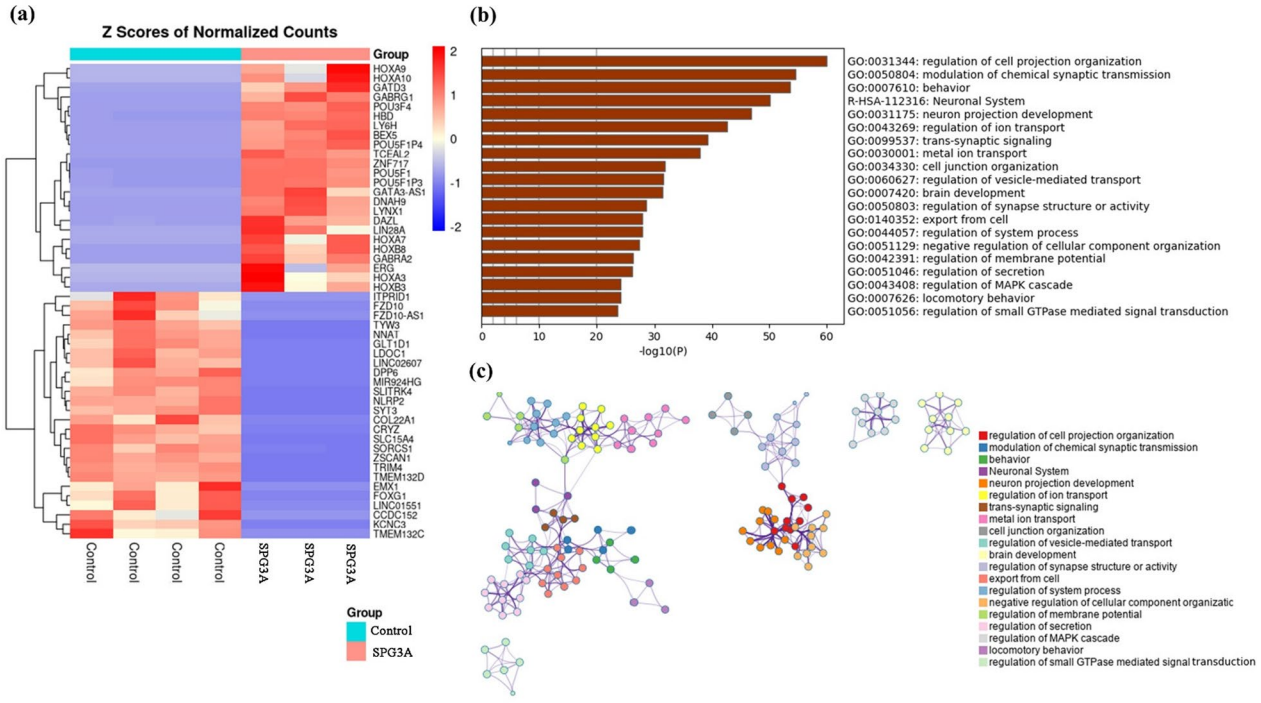

Fig. 1 mRNA sequencing reveals transcriptional dysregulation of important neurodevelopment related pathways in SPG3A cortical PN cultures. **a** Heatmap showing the top enriched terms across input gene lists. **b** Metascape bar graph of common downregulated pathways. SPG3A neurons exhibit major downregulation of pathways critical for neuronal development, including projection, synapse, and structure, colored by p-values. **c** Network analysis of enriched terms colored by cluster ID. Pathway and cluster network analyses revealed significant reduction of trans-synaptic signaling and chemical synaptic transmission in SPG3A neural cells

cast the tree into term clusters, and the representative terms from the full cluster were converted into a network layout (Fig. 1c). The network was visualized with Cytoscape, using a "force-directed" layout and with edge bundled for clarity. This comprehensive analysis revealed interactions between synaptic dysfunction and critical neuronal pathways including regulation of vesicle-mediated transport, regulation of membrane potential, and neuron projection development (Supplemental Tables 2 and 3). These data prefigure synaptic dysfunction in the pathogenesis in SPG3A, which is examined in detail in this study.

Characterization and neural differentiation of SPG3A iPSCs

To investigate the mechanisms and test the compounds in ATL1-mutated human neurons, we established iPSCs from a second patient with severe clinical phenotype [2] and a distinct mutation (p.Met408Thr). After culturing the patient fibroblast cells, reprogramming was induced by infecting these cells with Sendai virus containing pluripotent genes *Oct4, Sox2, L-Myc,* and *Klf4*. After infection, fibroblast cells changed their morphology and started to form small clones (Fig. 2a), and at around 3 weeks, distinct iPSC clones were observed. These clones were then picked, passaged and expanded to establish iPSC lines. To ensure the generated patient-specific SPG3A iPSCs retained their stem cell identity, we assessed their pluripotency potential at both the mRNA and protein levels (Fig. 2b and c). Immunofluorescence staining revealed robust expression of key pluripotency markers: OCT4, NANOG, SOX2, and SSEA4 (Fig. 2c). Real-time PCR (RT-PCR) further confirmed elevated levels of pluripotency marker genes *OCT4, SOX2,* and *NANOG* compared to the original patient fibroblasts. Additionally, fibroblast-enriched markers *FGF5, FGF8 and FGF9* were downregulated in iPSCs, indicative of successful reprogramming towards a pluripotent state (Fig. 2b). To further confirm the pluripotency in vivo, we

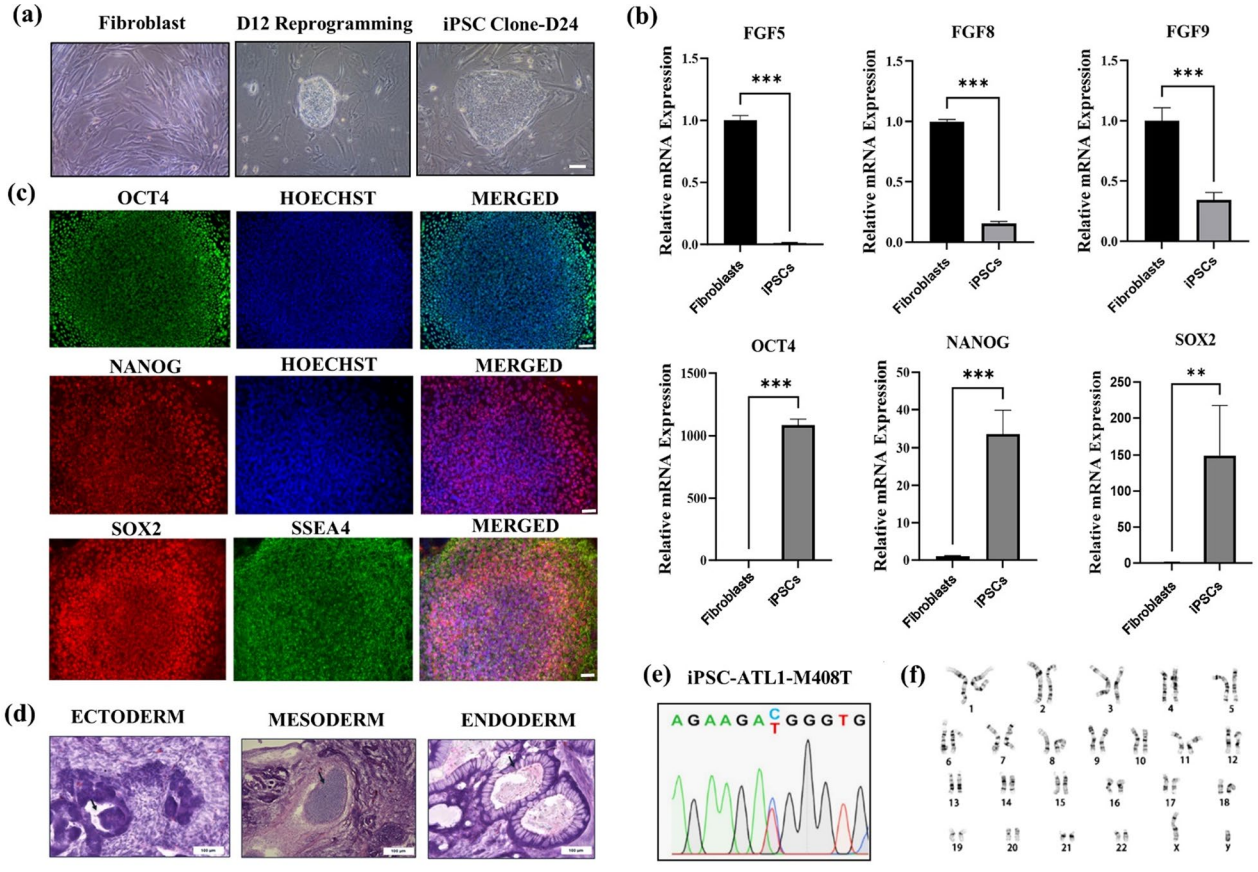

Fig. 2 Generation and characterization of patient-specific iPSCs. **a** Cultured fibroblast cells from a SPG3A patient show typical elongated morphology. Cells were then infected with Sendai virus, which started to form small colonies after about 2 weeks. **b** qRT-PCR showing the differential expression of fibroblast- and stem cell-related genes in fibroblast cells and reprogrammed iPSCs. **c** iPSCs colonies expressing ESC markers OCT4, NANOG, SSEA4, and SOX2 were imaged by immunofluorescence microscopy. Scale bars, 50 µm. **d** After injection into immune-deficiency mice, iPSCs formed teratomas with 3-germ layer structures on H&E staining, confirming pluripotency. **e** Validation of the mutation in SPG3A iPSCs; Sanger sequencing confirmed a heterozygous mutation at c.1223 T > C (p.M408T). **f** Normal karyotype was observed in iPSCs after multiple passages. Data are presented as Mean ± SD, n = 3. $^{**}p < 0.01$, $^{***}p < 0.001$ by two-sided *t*-test

performed teratoma assay, a golden standard method for testing the iPSCs. As seen in Fig. 2d, we observed that SPG3A teratomas consisted of neural cells (ectoderm), chondrocytes (mesoderm) and intestinal epithelium-like structures (endoderm). These data reveal that the iPSCs can generate structures of 3 germ layers in vivo, indicating the successful reprogramming of fibroblast cells into iPSCs.

To ensure the authenticity and accuracy of the patient-derived SPG3A iPSCs, we employed Sanger sequencing to examine the mutations (Fig. 2e) and performed karyotype analysis of the SPG3A iPSCs (Fig. 2f). This allowed us to confirm normal karyotype and the maintenance of patient-specific SPG3A mutations (i.e. p.Met408Thr) in the iPSCs. Further analysis of genomic DNA from iPSC clones showed no expression of Sendai viral vector sequences, indicating successful clearance of the virus (Supplemental Fig. 1). Finally, to confirm authenticity of the patient-derived SPG3A iPSC, we performed STR analysis and compared the reprogrammed iPSCs and fibroblast cells. The STR analysis confirmed that the iPSCs derived from both Patient 1 and Patient 2 retained the characteristic STR profile of the original donor fibroblast cell lines (Supplemental Table 4), establishing their suitability for studying the disease mechanisms in a controlled cellular model.

ATL1 mutations result in impaired lipid trafficking and aberrant synaptic organization in SPG3A

After successfully generating and characterizing patient-specific SPG3A iPSCs, we differentiated them into cortical projection neurons (PNs) to study the impact of Atlastin-1 mutations on the degeneration of these neurons. We employed established methods from previous studies to guide the transformation of hiPSCs into cortical PNs [8, 27] (Fig. 3a). Phase-contrast images were captured at each stage of the differentiation process to monitor the morphological changes and showed proper progression toward mature cortical PNs (Fig. 3b). Further, the differentiated cells were verified as cortical PNs by observing positive immunostaining for Ctip2 and Tau (Fig. 3c). Both control and SPG3A iPSCs efficiently differentiated into $CTIP2^{+}$ cortical PNs (Supplemental Fig. 2).

Following the differentiation of patient-specific cortical PNs, we sought to delve deeper into axonal defects associated with *ATL1* mutations, guided by insights from our mRNA-seq data on downregulated genes and pathways. We used cortical neurons derived from iPSCs of two SPG3A patients including patient 1 (PT1, ATL1-P342S) established previously and patient 2 established in this study (PT2, ATL1-M408T). As previously discussed, our unbiased sequencing data showing the alteration of lipid and synaptic pathways. To this end, we evaluated the expression of a representative group of genes linked to both synaptic and lipid trafficking in cortical PNs harboring ATL1-P342S and ATL1-M408T mutations. From our sequencing data, the most significantly changed pathways were cell projection organization, trans-synaptic organization, synapse plasticity, neuronal systems and lipid metabolism (Supplemental Table 2). We first examined the cholesterol-related gene expression levels in SPG3A cortical PNs compared to the control neurons. Lipoproteins, namely APOE, aid in the transfer of cholesterol from glial cells to neurons. Expression level of *APOE* in ATL1-P342S and ATL1-M408T cortical PNs was significantly decreased (Fig. 3d). Moreover, the expressions of *ABCA1, ABCA2*, and *ABCG1*, genes that involved in lipid and cholesterol trafficking were significantly reduced in ATL1-P342S and ATL1-M408T cortical PNs (Fig. 3d). This finding aligns with our mRNA sequencing findings, indicating a disruption in cholesterol homeostasis, and lipid metabolism in SPG3A neuronal culture.

Next, to examine the synaptic dysfunction in ATL1 mutated neurons, we evaluated synaptic-related genes *glutamate metabotropic receptor 1* (*GRM1)* and *SYNAPSIN* expression in SPG3A cortical PNs. *GRM1* and *SYNAPSIN* expression was significantly reduced in SPG3A cortical PNs at mRNA levels as compared to control (Fig. 3e). Both genes play an important role in synapse formation and organization. Additionally, we examined lipid droplet (LD)-related genes, as ATL1 has a known role in regulating LDs that store and regulate lipids. Analysis of gene expression data revealed that the mRNA expressions of the LD-related genes, *perilipin 2 (PLIN2)* and *perilipin 3 (PLIN3)*, were significantly reduced in SPG3A cortical PNs (Fig. 3f); PLIN2 is an LD protein that is universally expressed and regulates SREBF1, a gene critical for lipid and cholesterol metabolism [26, 29]. Taken together, this targeted analysis revealed a striking reduction in the expression of genes involved in synaptic, lipid, and cholesterol functions across both mutations, further supporting the implication of lipid and synaptic dysfunction in SPG3A.

LXR623 restores lipid trafficking and rescues Synapsin dysfunction in SPG3A cortical neural cells

How impaired lipid homeostasis leads to synaptic dysfunction, and what is the interplay between these processes in the degeneration of cortical PN axons in SPG3A? Our previous study showed that liver X receptor agonist (i.e., GW3965) can restore cholesterol homeostasis by regulating the lipid droplet and trafficking in SPG3A [29]. To dissect the role of lipid defects in synaptic dysfunction in SPG3A, here, we examined the effects of a lipid-targeting drug, LXR623 on SPG3A cortical PNs. LXR623 is a potent LXR agonist and orally available making it a promising candidate for future clinical development [49]. We first examined the effects of LXR623

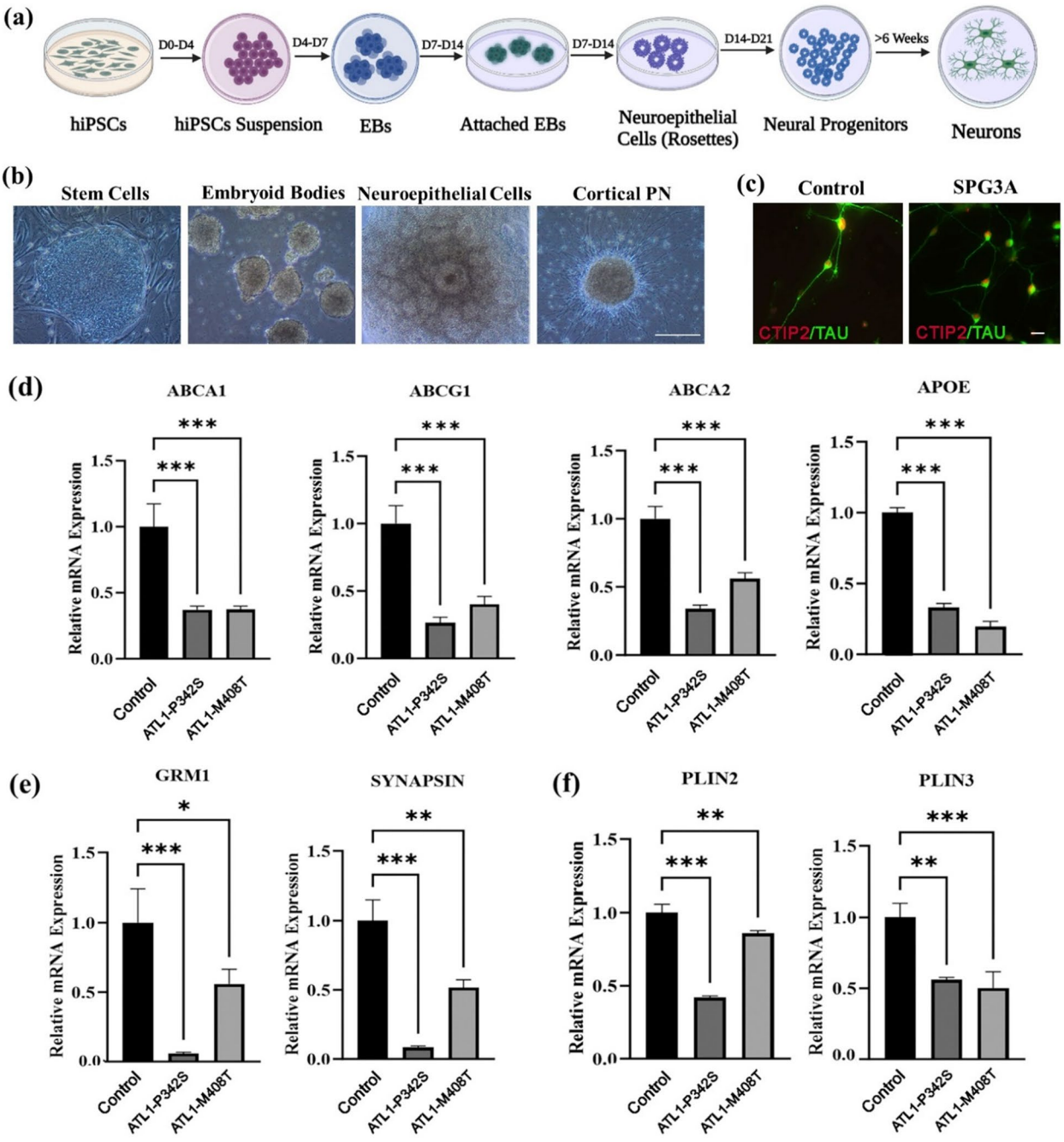

Fig. 3 Neural differentiation of iPSCs and altered lipid and synapsin-related genes in SPG3A. **a** Schematic diagram of the differentiation protocol for cortical PNs from iPSCs. **b** Phase contrast images show typical stages during differentiation of cortical PNs from hiPSCs. Scale bar, 200 µm. **c** Control and SPG3A iPSCs were differentiated into cortical PNs that stained positively with Ctip2 (red) and Tau (green). Scale bar, 20 µm. **d–f** qPCR analyses of control and SPG3A cortical PN cultures revealed significant reduction of genes involved in lipid and cholesterol trafficking (**d**), synapse organization (**e**), and lipid droplet formation (**f**). Data are presented as Mean ± SD, n = 3. *$p < 0.05$, **$p < 0.01$, *$p < 0.001$ versus control group by Dunnett's test after ANOVA

on synaptogenesis by analyzing synapsin 1 expression (Fig. 4a). Synapsin I is a synaptic vesicle associated protein, which is involved in regulating synaptogenesis and neurotransmitter release. We quantified the number of synapsin 1-positive clusters per 100 µm neurite length using ImageJ software (Fig. 4b). Our data reveal a significant reduction of synapsin-1 clusters in ATL1-P342S and ATL1-M408T cortical PNs compared to control neurons. Notably, treatment of LXR623 significantly increases synapsin numbers in SPG3A neurons, suggesting that targeting lipid defects can rescue the synaptic dysfunction.

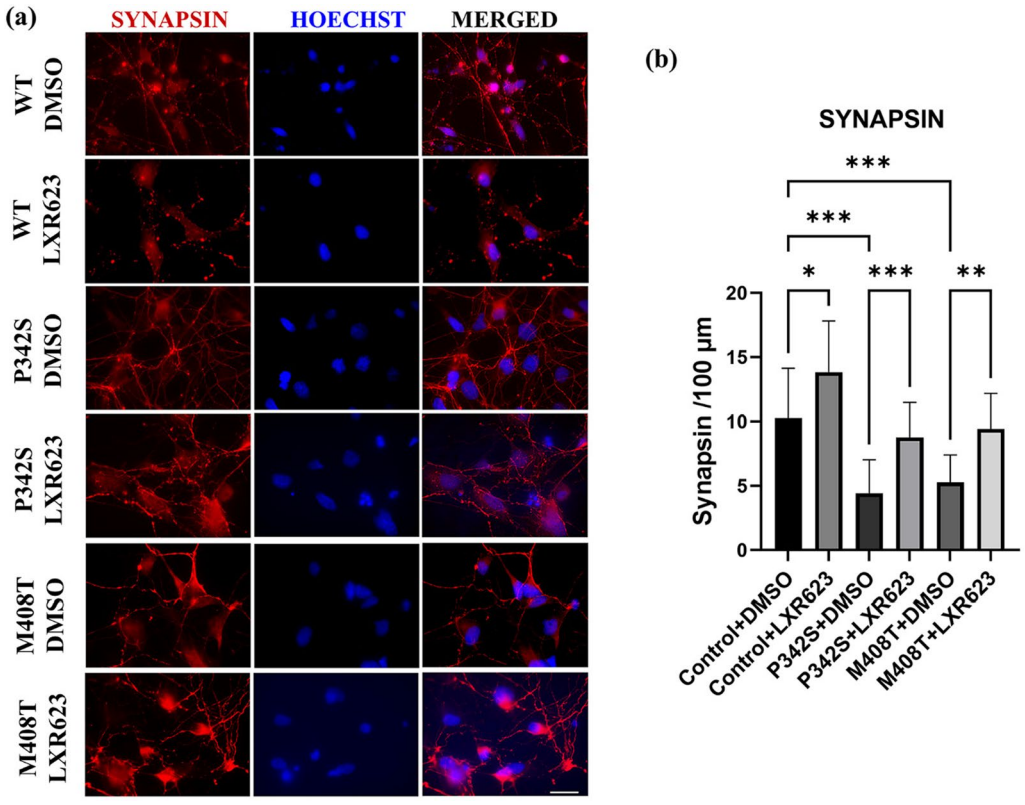

Fig. 4 LXR agonist treatment rescues synaptic defects in SPG3A cortical PNs. **a** Immunostaining of synapsin protein in cortical PN cultures derived from wild-type (WT) control and SPG3A iPSCs, with or without LXR623 treatment. Scale bar, 50 µm. **b** Quantifications of number of synapses per 100 µm neurite in control and SPG3A neurons treated with drug (LXR623) or vehicle control (DMSO). Three independent biological replicates for each group were analyzed. Data are represented as mean ± SD. *$p < 0.05$, **$p < 0.01$, ***$p < 0.001$ by Tukey's test after ANOVA

To further delineate the underlying mechanisms, we examined the expression of cholesterol efflux, LD, and synaptic genes after LXR623 treatment. Cortical PNs produced from *ATL1*-P342S and *ATL1*-M408T iPSCs showed substantial alterations in ER calcium ion balance and cholesterol efflux. SPG3A cortical PNs had decreased *ABCA1, ABCA2, ABCG1* expression. The mRNA expression level of *APOE*, a critical regulator of lipid and cholesterol transfer, was also significantly reduced in SPG3A neurons (Fig. 5a). After treatment with the LXR agonist, the expressions of these genes were significantly increased, reaching levels that were comparable to those measured in control neurons (Fig. 5a). Considering that atlastin-1 can directly modulate LDs, we then examined the expression of LD-related genes. Interestingly, mRNA expression of *PLIN2* and *PLIN3*, critical LD genes, were significantly reduced in SPG3A cortical PNs, which are mitigated by the LXR623 treatment (Fig. 5b). Further, we examined the synapse-related gene expression at the mRNA level in ATL1 mutant neurons compared to the control group including *SYNAPSIN* and *GRM1*. Previously, we found that *GRM1* and *SYNAPSIN* expressions were significantly reduced in SPG3A cortical PNs (Fig. 3e). After LXR623 treatment, the expressions of *SYNAPSIN* as well as *GRM1*, critical factors for the formation and organization of synapses, were significantly increased in the SPG3A cortical PNs as compared to SPG3A neurons treated with DMSO (Fig. 5c). Taken together, our results reveal that restoring LD and cholesterol pathways using an LXR agonist can effectively mitigate synaptic dysfunction in SPG3A, implicating of impaired lipid homeostasis in synaptic dysfunction and providing a potential therapeutic target for SPG3A.

LXR623 ameliorated synaptic dysfunction and cholesterol trafficking deficits caused by ATL1 mutation

To examine the cause-effect relationship between SPG3A mutations and synaptic deficits, we generated cortical PNs from ATL1-P342S and an isogenic control iPSC line (Fig. 6). To confirm the pluripotency of the corrected cell line, stem cell colonies were stained for pluripotency markers OCT4, SOX2, and SSEA4 (Supplemental Fig. 3a). We also performed karyotype analysis to confirm genomic integrity (Supplemental Fig. 3b). The western blot analysis showed decreased synapsin protein levels in the *ATL1*-mutant neurons, suggesting impairments in synapse formation or maintenance of these cells (Supplemental Fig. 4a and b). Furthermore, synapsin levels were

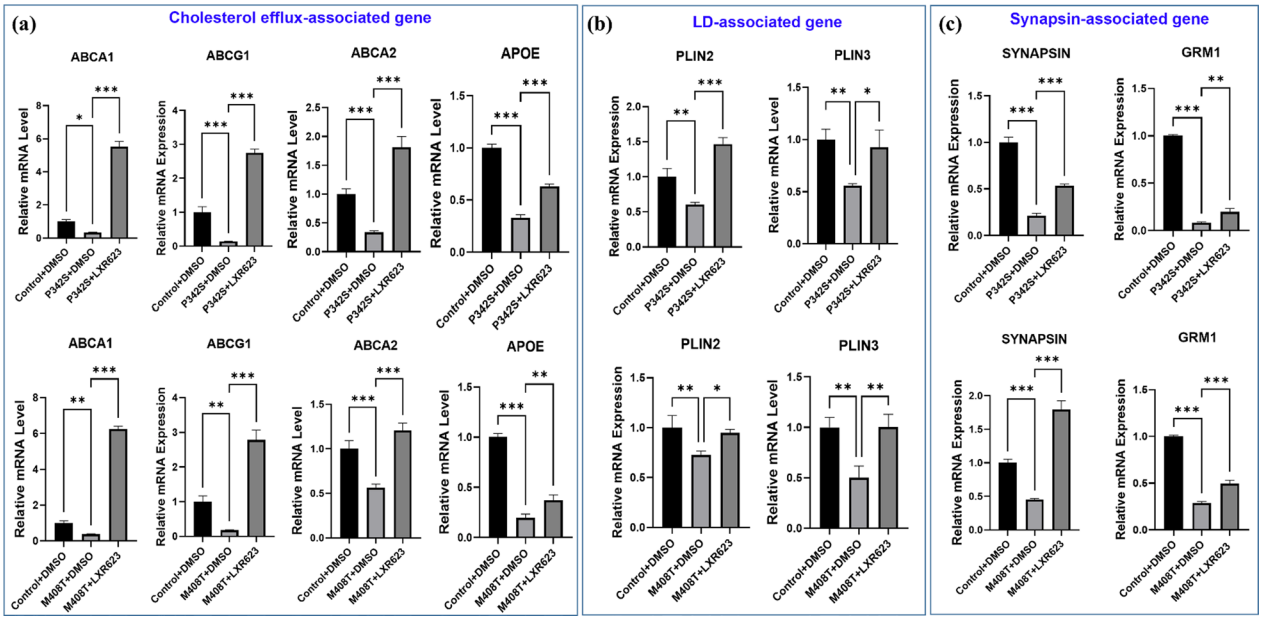

Fig. 5 The effects of LXR623 on the expression of critical genes in lipid and synaptic pathways. **a** qPCR showing the significant increased expression of lipid and cholesterol trafficking genes (*ABCA1*, *ABCA2*, *ABCG1*, *APOE*) after the treatment of LXR623 in both ATL1-P342S and AL1-M408T cortical cells. **b** The expressions of lipid droplet related genes (*PLIN2* and *PLIN3*) were significantly increased in LXR623-treated cells compared to that in DMSO (vehicle control)-treated group. **c** LXR623 treatment significantly increased expression of *GRM1* and *SYNAPSIN* in *ATL1*-mutated cortical PN cultures, suggesting the restoration of lipid and synaptic pathways by LXR623. Data are presented as mean ± SD, n = 3. *$p < 0.05$, **$p < 0.01$, ***$p < 0.001$ versus ATL1-mutated (P342S or M408T) DMSO group by Dunnett's test after ANOVA

increased after treatment with LXR623, further confirming the protective effects of LXR623 for synaptic functions in SPG3A neurons. Next, an analysis of synapse density, as indicated by synapsin expression through immunofluorescence microscopy, revealed a significant reduction of synaptic density in patient neurons compared to isogenic controls (Fig. 6a), further supported by analyzing synapse number per 100 µm neurite length and quantified by ImageJ software (Fig. 6b). The synaptic deficit was also confirmed using synapsin ELISA, which suggests that there is a comparable reduction of synapse proteins in both groups (ATL1-P342S & ATL1-M408T) (Supplemental Fig. 4c and d). Moreover, synapsin proteins were increased after treatment with LXR623 (Supplemental Fig. 4), further confirming the protective effects of LXR623 for synaptic functions in SPG3A neurons.

Next, to determine the functionality of the neurons, we performed calcium imaging and compared the calcium activity between ATL1-P342S and isogenic control neurons before and after stimulation with glutamic acid (Fig. 6d). Interestingly, calcium imaging analysis indicated that the calcium activity was significantly reduced in patient-derived neurons as compared to isogenic controls (Fig. 6e). Both the basic levels of the calcium activity (before stimulation) and calcium levels after stimulation were significantly reduced in ATL1-P342S neurons (Fig. 6e). Together with the alterations in synaptic protein expression, these data suggest a compromised capacity for external signal transmission indicative of synaptic dysfunction [1]. Moreover, treatment with LXR623 significantly increased cytosolic calcium levels in *ATL1*-mutated neurons (Fig. 6d and e), further supporting the increased synapsin activity and improved calcium homeostasis by LXR623 in patient-derived cortical PNs. Taken together, our data suggest that synaptic activity is impaired in the SPG3A patient neurons and can be mitigated by LXR623 treatment.

How does LXR623 affect the synaptic functions in SPG3A neurons, and what is the interplay between the lipid deficits and synaptic function? Our previous study has reported cholesterol trafficking deficits in SPG3A astrocytes. Astrocytes have a critical role in synaptic function, and neurons depend on cholesterol from glial cells, especially astrocytes. This brings up the possibility that LXR623 can regulate cholesterol trafficking from astrocytes to neurons, improving synaptic functions. To test this possibility, we generated astrocytes from ATL1-P342S and control iPSCs using our well-established protocol [29]. We then labelled these astrocytes and compared cholesterol efflux between SPG3A and control neurons. Results indicated a significant reduction of cholesterol efflux from ATL1-P342S astrocytes compared to control astrocytes (Supplemental Fig. 5). Moreover, the reduced cholesterol efflux is significantly mitigated after the treatment with LXR623, suggesting

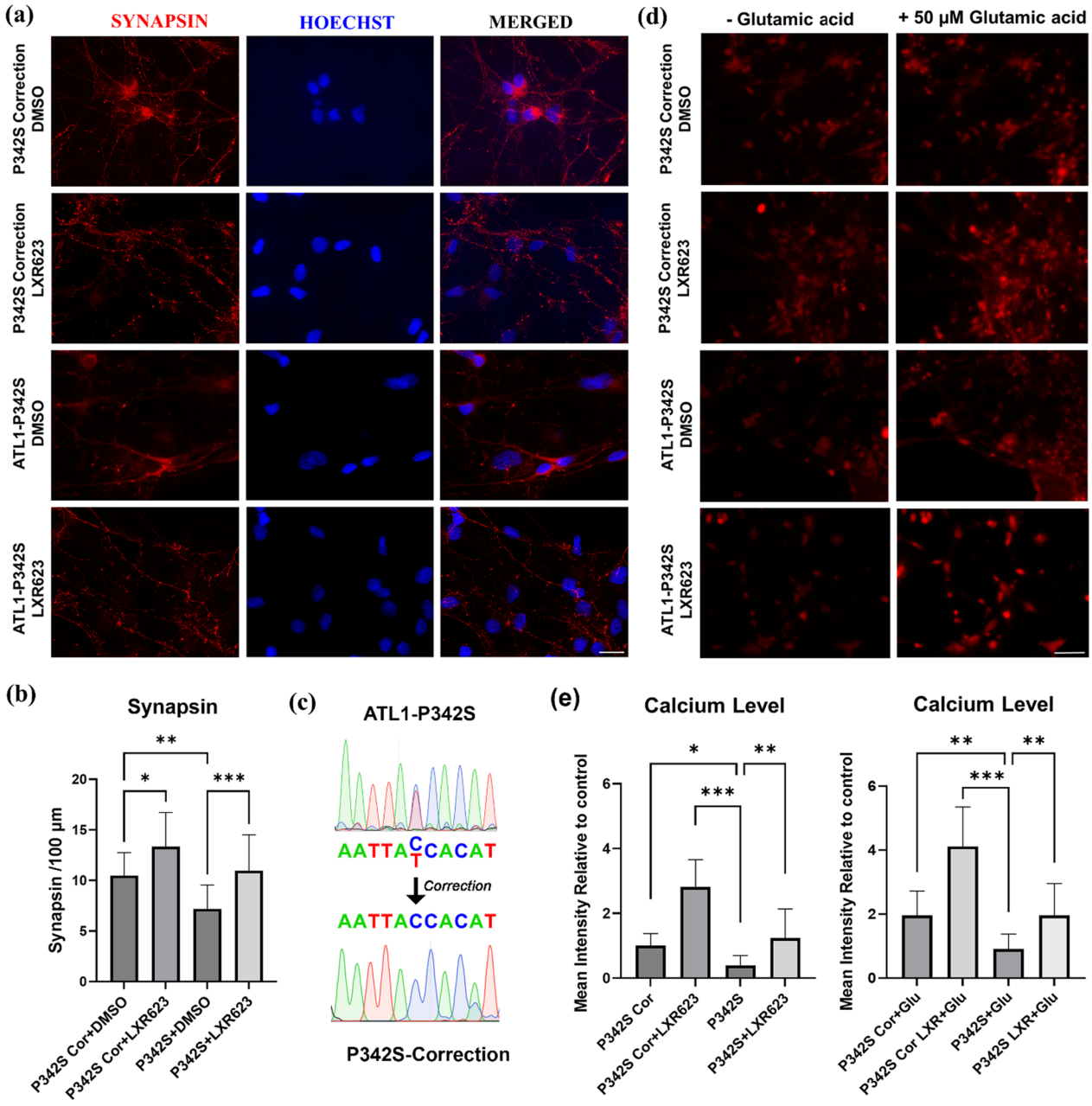

Fig. 6 LXR623 treatment rescues Synapse Dysfunction and Calcium Dynamics in SPG3A isogenic cell lines. **a** Synapsin protein expression in SPG3A mutant and isogenic cortical PNs treated with 1 µM LXR623. Scale bar, 20 µm. **b** Quantification of synapse per 100 µm neurite length reveals a significant reduction in synapsin expression in SPG3A mutant neurons compared to an isogenic control. **c** Correction of point mutations in SPG3A iPSCs to generate isogenic control iPSCs. **d** Changes in intracellular calcium levels in SPG3A mutant and isogenic control neurons visualized using X-rhod-1 AM. Fluorescence intensity was measured at baseline and following stimulation with glutamic acid (50 µM). Scale bar, 50 µm. **e** The effect of LXR623 pretreatment (1 µM, 1 week) on calcium activity was assessed at baseline (left panel) and after stimulation (right panel). Quantification of calcium levels (relative to isogenic control baseline) indicates significant effects of LXR623 on calcium. Three independent biological replicates for each group were analyzed. Data are presented as Mean ± SD. *$p < 0.05$, **$p < 0.01$, ***$p < 0.001$ by Tukey's test after ANOVA

that LXR623 exerts protective effects on synaptic function through regulating the cholesterol trafficking. The dynamic changes of calcium and synaptic activities and detailed mechanisms by which the interplay of neurons and glial cells in the pathogenesis of SPG3A await further examination.

LXR623 effectively mitigates axonal swellings and apoptosis in long-term cultures of SPG3A

To determine the role of lipid and synaptic defects in the degeneration of SPG3A cortical PNs, we examined the efficacy of targeting these defects against nerve degeneration in long-term cultures. LXR623 is a synthetic

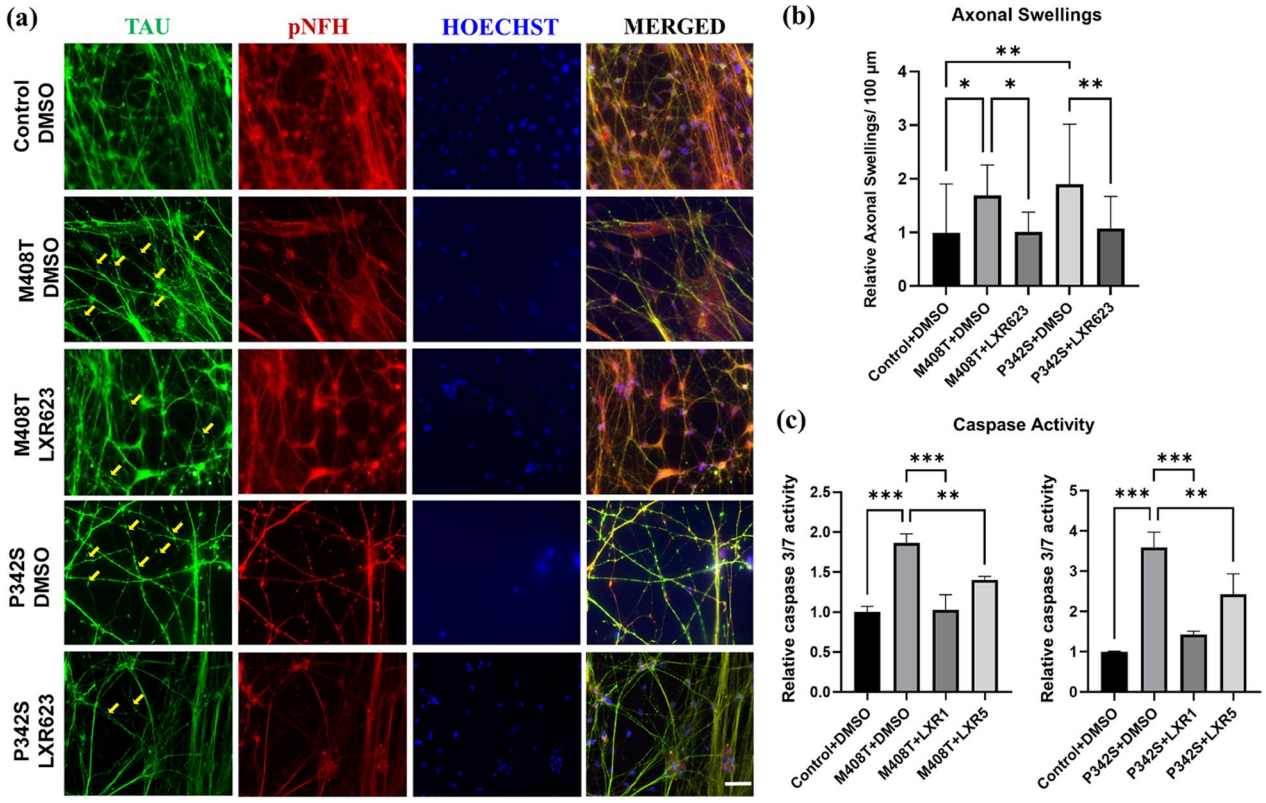

Fig. 7 LXR623 mitigates the axonal swellings and apoptosis in SPG3A long-term cultures. **a** Immunostaining of in healthy control derived and SPG3A cortical PNs, with and without LXR623. Immunostaining of Tau showing the formation of axonal swellings along axons in *ATL1* mutant cortical PNs; Scale bar, 50 µm. **b** Quantification revealed a significant increase in the density of axonal swellings in *ATL1* mutant neurons compared to control. Three independent biological replicates for each group were analyzed. Data were presented as mean ± SD. $^{**}p < 0.01$ versus SPG3A DMSO group by Tukey's test after ANOVA. **c** Apoptosis levels as indicated by relative Caspase 3/7 activity were analyzed in both ATL1-mutated cortical PNs after being treated with LXR623 (1 µM and 5 µM) or vehicle control (DMSO). The Caspase 3/7 activities were significantly increased in ATL1-mutated groups, which were effectively mitigated after treatment with LXR623 at both doses. Data were presented as mean ± SD, n=3. $^{**}p < 0.01$, $^{***}p < 0.001$ versus ATL1-mutated DMSO group by Dunnett's test after ANOVA

molecule that activates LXRs, which is an important regulator of cholesterol metabolism and trafficking. Using patient iPSC-derived neurons, we observed the rescue of synaptic dysfunction in SPG3A (Figs. 4 and 6). Importantly, LXR623 can traverse the blood–brain-barrier and has proven to be safe in a phase I human clinical study [49], making it an ideal candidate for future therapeutic applications. We examined the effect of LXR623 on the axonal degeneration by analyzing axonal swellings in SPG3A cortical PNs in long-term cultures (3 months). Axonal swellings are a characteristic pathological change observed in cell and animal models of HSP, which is caused by the accumulation of transported cargos as a result of impaired transport. We have previously shown the increased axonal swellings in ATL1-P342S neurons [29]. Here, we compared the axonal swellings between control and SPG3A ATL1mutant neurons. Tau immunostaining was performed to visualize axonal swellings in ATL1-mutated neurons (Fig. 7a). There is a significant increase in the axonal swelling density in ATL1-mutated neurons compared to control (Fig. 7b). Interestingly, after the treatment of LXR623 (1 µM), the axonal swelling density in ATL1-M408T and ATL1-P342S neurons was significantly reduced, revealing the protective effects of LXR623 against axonal degeneration.

Furthermore, we examined the effects of LXR623 on apoptosis levels to investigate the protective impact of this drug on SPG3A cortical PNs. The apoptosis levels as indicated by relative Caspase 3/7 activity was significantly increased in SPG3A neurons compared to control neurons (Fig. 7c). The administration of LXR623 resulted in a significant decrease in Caspase 3/7 levels in the SPG3A group compared to that in the control treated with DMSO. Both 1 µM and 5 µM can significantly reduce the apoptosis, validating the protective effects of LXR623 in SPG3A cortical PNs. Collectively, our findings demonstrate that LXR623 treatment, which restores lipid and synaptic function, can effectively mitigate the axonal and neuronal degeneration of SPG3A neurons in long-term cultures, highlighting the importance of targeting these defects for therapeutic interventions in HSP.

Discussion

Lipid dysfunction is an emerging pathologic change involved in neurodegenerative diseases including HSP, though the interplay between lipids and synaptic defects, and the targeting of these defects to effectively mitigate axonal degeneration, remain to be elucidated. Here, we demonstrate that SPG3A mutations in *ATL1* impair lipid trafficking and synaptic pathways, disrupting synaptogenesis and leading to axonal degeneration and apoptosis of SPG3A cortical neurons. Notably, using patient-specific iPSC-derived cortical neurons from two SPG3A patients with distinct mutations and clinical presentations, we tested the protective effects of an oral LXR agonist, LXR623. LXR623 significantly mitigated the reduction in synaptic proteins and the accumulated axonal swellings, revealing its protective role against synaptic defects and axonal degeneration. Further analyses confirmed the effect of LXR623 on rescuing the lipid trafficking and LD pathway, which correlated with the improvement of synaptogenesis and nerve degeneration. Moreover, LXR623 also inhibits apoptosis in the mutant neurons, further supporting its protective effects and providing a promising therapeutic approach for SPG3A.

The *ATL1* protein atlastin-1 localizes to the tubular ER and has a critical role in the organization of ER three-way junctions. Atlastin-1 interacts with several other HSP proteins including spastin (SPG4) and REEP1 (SPG31), forming protein complexes within the tubular ER membrane [35]. Mutations of these HSP genes, which accounts for about 50% of the HSP cases, led to impaired ER morphogenesis, implicating ER and lipid defects in the pathogenesis of HSP [46]. Though lipid dysfunction has been observed in patient iPSC-derived neural cells, how lipid defects result in the dysfunction and degeneration of cortical PNs remain elusive. Our unbiased genomic studies comparing SPG3A and control neural cells identified synaptic dysfunction as a top affected pathway in addition to the aberrant lipid pathways. Given that lipids have an important role in synaptogenesis, synaptic dysfunction may be a critical, downstream pathologic change in SPG3A. We further examined synaptic defects in neural cells derived from iPSCs of two patients with distinct *ATL1* mutations. *ATL1* mutations impair the expression of *SYNAPSIN1* and *GRM1*, which are critical for synapse formation and neurotransmitter release, confirming synaptic dysfunction in *ATL1*-mutated human neural cells. Moreover, treatment of SPG3A cells with a lipid-targeting compound (i.e., an LXR agonist) significantly mitigated the aberrant synaptogenesis, implicating lipid defects in the synapse dysfunction observed in SPG3A.

Treatment with LXR623 leads to a robust increase in calcium activity under baseline conditions and in response to glutamic acid treatment in SPG3A patient-derived neurons. These results suggest that LXR623 potentiates synaptic activity in SPG3A neurons, though the detailed dynamic changes of calcium activity need further investigation. The impaired calcium activity coincides with the reduced synaptic puncta observed in SPG3A PNs, and both impairments are significantly ameliorated by LXR623 treatment. These findings indicate that LXR623 may be a potential therapeutic agent for SPG3A through the rescue of synaptic dysfunction. Given the critical role of astrocytes in synaptic function and cholesterol homeostasis of neurons, we also generated a pure population of astrocytes and compared cholesterol trafficking between *ATL1*-mutated and isogenic control astrocytes. Mitigation of cholesterol efflux impairments by LXR623 in *ATL1*-mutated astrocytes revealed the implications of impaired lipid trafficking in synaptic deficits, though detailed mechanisms by which *ATL1* mutations affect calcium signaling and synaptic activity await further investigation. It will also be interesting to dissect the specific role of astrocytes in regulating synaptic function in the future, through co-culturing ChR2-labeled astrocytes with neurons and examining the dynamic responses of neurons upon the specific stimulation of astrocytes.

SPG3A is the most common early-onset form of HSP and results from *ATL1* missense mutations that span different sites broadly throughout the *ATL1* gene. A recent meta-analysis of the mutations found that de novo mutations usually led to more severe phenotypes [2]. Specifically, ATL1-M408T de novo mutations are prominently associated with more severe and extensive symptoms. Similar to patient 2 (ATL1-M408T), patient 1 (ATL1-P342S) also harbors a de-novo mutation, with early onset of symptoms at the age of 2 [55]. Both ATL1-P342S and ATL1-M408T iPSC-derived cortical neurons exhibited significant reductions in synaptic proteins and functions. Whether the disease progression caused by these two mutations will show differences, and whether the effects of these two mutations on other types of neurons that are responsible for complicated symptoms are different, will be interesting to examine in the future.

A characteristic pathologic change observed in multiple forms of HSP is increased axonal swellings caused by impaired transport and accumulated transported cargos [14, 22]. We have found accumulated axonal swellings in SPG3A iPSC-derived neuron cultures, which is mitigated by LXR623. The protective effects of LXR623 are further supported by its potency in reducing apoptosis, which can be caused by lipid and synaptic defects [50]. Recent studies have reported the involvement of double strand DNA damage, which is a major cause of apoptosis, in HSP [5, 39, 44]. Interestingly, we have observed double strand DNA break repair in the upregulated pathways (Supplemental Table 3), prefiguring DNA damage in SPG3A. The detailed mechanisms underlying

double strand DNA damage and the interplay between these pathological processes in SPG3A await further investigation.

Currently, HSP treatments are symptomatic, ranging from physical therapy and oral anti-spasmodic medications to botulin toxin injections and even various surgeries for disease management depending on the complexity of symptoms [4, 43]. There remains a lack of effective approaches to directly target axonal degeneration and nerve dysfunction. Using patient-specific iPSC-derived neurons with two distinct mutations, our study revealed the protective effects of LXR623 against synaptic dysfunction, axonal degeneration and apoptosis in these SPG3A neurons. LXR623 is a potent and oral-active agonist of LXRs. LXR623 can cross the blood–brain barrier and has been shown to be safe in clinical trials [23, 49]. By providing evidence for the potential of LXR623 in alleviating neurodegeneration, this study opens new avenues for exploring novel therapeutic approaches for SPG3A and potentially other forms of HSP. Additionally, it will be interesting to further investigate the long-term effects and efficacy of LXR623 treatment using in vivo models, which will be crucial for advancing its therapeutic potential.

Conclusion

By combining iPSC modeling and non-biased RNA sequencing, this study identifies synaptic dysfunction as a top-altered pathway in SPG3A. Our data further demonstrate the role of synaptic dysfunction in the degeneration of SPG3A neurons. The application of LXR623, an oral active LXR agonist that regulates lipid trafficking, effectively mitigates synaptic deficits and the degeneration of human cortical neurons, providing a promising therapeutic approach for SPG3A.

Abbreviations

ANOVA	Analysis of variance
ApoE	Apolipoprotein E
ATL1	Atlastin-1
ER	Endoplasmic reticulum
GRM1	Glutamate metabotropic receptor 1
HSPs	Hereditary spastic paraplegias
iPSCs	Induced pluripotent stem cells
LD	Lipid droplet
LXR	Liver-X-receptor
MEF	Mouse embryonic fibroblast
NDM	Neural differentiation medium
PLIN2	Perilipin 2
PLIN3	Perilipin 3
PNs	Projection neurons

Supplementary Information

The online version contains supplementary material available at https://doi.org/10.1186/s40478-025-02134-5.

Supplementary Material 1. Supplemental Figures 1 to 5.

Supplementary Material 2. Supplemental Tables 1 to 4.

Acknowledgements

We would like to acknowledge the Northwestern University Sequencing core for performing mRNA-sequencing analysis.

Author contributions

XJL and CB conceived and designed the experiments. GT, RD, YM, PK, AK, and ZC performed experiments and acquired data. SS, JEA and DEF provided patient cell lines. GT, RD, YM, PK, AK, ZC, and XJL analyzed the data. GT and XJL wrote the manuscript with inputs from CB, RD, YM, PK, AK, DEF, ZC. All authors approved the final version and the submission of the manuscript.

Funding

This study is supported by the Carter Foundation for Neurologic Research (to XJL), National Institutes of Health grant (R01NS118066, to XJL), the Master of Science in Medical Biotechnology Program at the University of Illinois College of Medicine Rockford (to RD, PK and AK), and the Massachusetts General Hospital (to CB). Research in the Ebrahimi-Fakhari Laboratory is supported by the Spastic Paraplegia Foundation, the Boston Children's Hospital Translational Research Program, and the National Institutes of Health/National Institute of Neurological Disorders and Stroke (K08NS123552).

Data availability

Data that support the findings of this study are available in the paper or from the corresponding author upon reasonable request.

Declarations

Ethics approval and consent to participate

All experiments involving iPSCs have been approved by the Institutional Biosafety Committee of the University of Illinois. Skin punch biopsies were obtained following a clinical research procedure (protocols #IRB-P00016199, #IRB-P00033016) authorized by the Institutional Review Board at Boston Children's Hospital.

Consent for publication

Not applicable.

Competing interests

The authors declare that they have no competing financial interests.

Received: 17 June 2025 / Accepted: 22 September 2025
Published online: 17 November 2025

References

1. Aggarwal A, Liu R, Chen Y, Ralowicz AJ, Bergerson SJ, Tomaska F, Mohar B, Hanson TL, Hasseman JP, Reep D et al (2023) Glutamate indicators with improved activation kinetics and localization for imaging synaptic transmission. Nat Methods 20:925–934. https://doi.org/10.1038/s41592-023-01863-6
2. Alecu JE, Saffari A, Jordan C, Srivastava S, Blackstone C, Ebrahimi-Fakhari D (2023) De novo variants cause complex symptoms in HSP-ATL1 (SPG3A) and uncover genotype-phenotype correlations. Hum Mol Genet 32:93–103. https://doi.org/10.1093/hmg/ddac182
3. Allen JA, Halverson-Tamboli RA, Rasenick MM (2007) Lipid raft microdomains and neurotransmitter signalling. Nat Rev Neurosci 8:128–140. https://doi.org/10.1038/nrn2059
4. Bellofatto M, De Michele G, Iovino A, Filla A, Santorelli FM (2019) Management of hereditary spastic paraplegia: a systematic review of the literature. Front Neurol 10:3. https://doi.org/10.3389/fneur.2019.00003
5. Bermudez-Guzman L, Leal A (2019) DNA repair deficiency in neuropathogenesis: when all roads lead to mitochondria. Transl Neurodegener 8:14. https://doi.org/10.1186/s40035-019-0156-x
6. Blackstone C (2018) Converging cellular themes for the hereditary spastic paraplegias. Curr Opin Neurobiol 51:139–146. https://doi.org/10.1016/j.conb.2018.04.025
7. Blackstone C, O'Kane CJ, Reid E (2011) Hereditary spastic paraplegias: membrane traffic and the motor pathway. Nat Rev Neurosci 12:31–42. https://doi.org/10.1038/nrn2946

8. Boisvert EM, Denton K, Lei L, Li XJ (2013) The specification of telencephalic glutamatergic neurons from human pluripotent stem cells. J Vis Exp. https://doi.org/10.3791/50321.10.3791/50321
9. Camargo N, Smit AB, Verheijen MH (2009) SREBPs: SREBP function in glia–neuron interactions. FEBS J 276:628–636
10. Chen Z, Chai E, Mou Y, Roda RH, Blackstone C, Li XJ (2022) Inhibiting mitochondrial fission rescues degeneration in hereditary spastic paraplegia neurons. Brain 145:4016–4031. https://doi.org/10.1093/brain/awab488
11. Cheng HT, Dauch JR, Porzio MT, Yanik BM, Hsieh W, Smith AG, Singleton JR, Feldman EL (2013) Increased axonal regeneration and swellings in intraepidermal nerve fibers characterize painful phenotypes of diabetic neuropathy. J Pain 14:941–947. https://doi.org/10.1016/j.jpain.2013.03.005
12. Christopherson KS, Ullian EM, Stokes CCA, Mullowney CE, Hell JW, Agah A, Lawler J, Mosher DF, Bornstein P, Barres BA (2005) Thrombospondins are astrocyte-secreted proteins that promote CNS synaptogenesis. Cell 120:421–433. https://doi.org/10.1016/j.cell.2004.12.020
13. Cui M, Tang X, Christian WV, Yoon Y, Tieu K (2010) Perturbations in mitochondrial dynamics induced by human mutant PINK1 can be rescued by the mitochondrial division inhibitor mdivi-1. J Biol Chem 285:11740–11752. https://doi.org/10.1074/jbc.M109.066662
14. Denton KR, Xu C, Shah H, Li XJ (2016) Modeling axonal defects in hereditary spastic paraplegia with human pluripotent stem cells. Front Biol (Beijing) 11:339–354. https://doi.org/10.1007/s11515-016-1416-0
15. Dottori M, Li WJ, Minchiotti G, Rosa A, Sangiuolo F (2023) Editorial: Reviews in induced pluripotent stem cells. Front Cell Dev Biol 11:1197891. https://doi.org/10.3389/fcell.2023.1197891
16. Fink JK (2006) Hereditary spastic paraplegia. Curr Neurol Neurosci Rep 6:65–76
17. Finsterer J, Loscher W, Quasthoff S, Wanschitz J, Auer-Grumbach M, Stevanin G (2012) Hereditary spastic paraplegias with autosomal dominant, recessive, X-linked, or maternal trait of inheritance. J Neurol Sci 318:1–18. https://doi.org/10.1016/j.jns.2012.03.025
18. Göritz C, Thiebaut R, Tessier LH, Nieweg K, Moehle C, Buard I, Dupont JL, Schurgers LJ, Schmitz G, Pfrieger FW (2007) Glia-induced neuronal differentiation by transcriptional regulation. Glia 55:1108–1122. https://doi.org/10.1002/glia.20531
19. Hazan J, Fonknechten N, Mavel D, Paternotte C, Samson D, Artiguenave F, Davoine CS, Cruaud C, Durr A, Wincker P et al (1999) Spastin, a new AAA protein, is altered in the most frequent form of autosomal dominant spastic paraplegia. Nat Genet 23:296–303. https://doi.org/10.1038/15472
20. Jacquet AD, Denis HL, Cicchetti F, Alpaugh M (2021) Current and future applications of induced pluripotent stem cell-based models to study pathological proteins in neurodegenerative disorders. Mol Psychiatr 26:2707–2707. https://doi.org/10.1038/s41380-021-01055-8
21. Jessen KR (2004) Glial cells. Int J Biochem Cell Biol 36:1861–1867. https://doi.org/10.1016/j.biocel.2004.02.023
22. Kasher PR, De Vos KJ, Wharton SB, Manser C, Bennett EJ, Bingley M, Wood JD, Milner R, McDermott CJ, Miller CC et al (2009) Direct evidence for axonal transport defects in a novel mouse model of mutant spastin-induced hereditary spastic paraplegia (HSP) and human HSP patients. J Neurochem 110:34–44. https://doi.org/10.1111/j.1471-4159.2009.06104.x
23. Katz A, Udata C, Ott E, Hickey L, Burczynski ME, Burghart P, Vesterqvist O, Meng X (2009) Safety, pharmacokinetics, and pharmacodynamics of single doses of LXR-623, a novel liver X-receptor agonist, in healthy participants. J Clin Pharmacol 49:643–649. https://doi.org/10.1177/0091270009335768
24. Klemm RW, Norton JP, Cole RA, Li CS, Park SH, Crane MM, Li L, Jin D, Boye-Doe A, Liu TY et al (2013) A conserved role for atlastin GTPases in regulating lipid droplet size. Cell Rep 3:1465–1475. https://doi.org/10.1016/j.celrep.2013.04.015
25. Krencik R, Weick JP, Liu Y, Zhang ZJ, Zhang SC (2011) Specification of transplantable astroglial subtypes from human pluripotent stem cells. Nat Biotechnol 29:528–534. https://doi.org/10.1038/nbt.1877
26. Lee M, Moon Y, Lee S, Lee C, Jun Y (2019) Ergosterol interacts with Sey1p to promote atlastin-mediated endoplasmic reticulum membrane fusion in *Saccharomyces cerevisiae*. FASEB J 33:3590–3600. https://doi.org/10.1096/fj.201800779RR
27. Li XJ, Zhang X, Johnson MA, Wang ZB, Lavaute T, Zhang SC (2009) Coordination of sonic hedgehog and Wnt signaling determines ventral and dorsal telencephalic neuron types from human embryonic stem cells. Development 136:4055–4063. https://doi.org/10.1242/dev.036624
28. Meijer IA, Dion P, Laurent S, Dupre N, Brais B, Levert A, Puymirat J, Rioux MF, Sylvain M, Zhu PP et al (2007) Characterization of a novel SPG3A deletion in a French-Canadian family. Ann Neurol 61:599–603. https://doi.org/10.1002/ana.21114
29. Mou Y, Dong Y, Chen Z, Denton KR, Duff MO, Blackstone C, Zhang SC, Li XJ (2020) Impaired lipid metabolism in astrocytes underlies degeneration of cortical projection neurons in hereditary spastic paraplegia. Acta Neuropathol Commun 8:214. https://doi.org/10.1186/s40478-020-01088-0
30. Namekawa M, Ribai P, Nelson I, Forlani S, Fellmann F, Goizet C, Depienne C, Stevanin G, Ruberg M, Durr A et al (2006) SPG3A is the most frequent cause of hereditary spastic paraplegia with onset before age 10 years. Neurology 66:112–114. https://doi.org/10.1212/01.wnl.0000191390.20564.8e
31. Nelakanti RV, Kooreman NG, Wu JC (2015) Teratoma formation: a tool for monitoring pluripotency in stem cell research. Curr Protoc Stem Cell Biol 32:4A 8 1-4A 8 17. https://doi.org/10.1002/9780470151808.sc04a08s32
32. Nieweg K, Schaller H, Pfrieger FW (2009) Marked differences in cholesterol synthesis between neurons and glial cells from postnatal rats. J Neurochem 109:125–134. https://doi.org/10.1111/j.1471-4159.2009.05917.x
33. Novarino G, Fenstermaker AG, Zaki MS, Hofree M, Silhavy JL, Heiberg AD, Abdellateef M, Rosti B, Scott E, Mansour L et al (2014) Exome sequencing links corticospinal motor neuron disease to common neurodegenerative disorders. Science 343:506–511. https://doi.org/10.1126/science.1247363
34. Orso G, Pendin D, Liu S, Tosetto J, Moss TJ, Faust JE, Micaroni M, Egorova A, Martinuzzi A, McNew JA et al (2009) Homotypic fusion of ER membranes requires the dynamin-like GTPase atlastin. Nature 460:978–983. https://doi.org/10.1038/nature08280
35. Park SH, Zhu PP, Parker RL, Blackstone C (2010) Hereditary spastic paraplegia proteins REEP1, spastin, and atlastin-1 coordinate microtubule interactions with the tubular ER network. J Clin Invest 120:1097–1110. https://doi.org/10.1172/JCI40979
36. Pfrieger FW (2003) Role of cholesterol in synapse formation and function. BBA-Biomembr 1610:271–280. https://doi.org/10.1016/S0005-2736(03)00024-5
37. Pfrieger FW, Ungerer N (2011) Cholesterol metabolism in neurons and astrocytes. Prog Lipid Res 50:357–371. https://doi.org/10.1016/j.plipres.2011.06.002
38. Piomelli D, Astarita G, Rapaka R (2007) A neuroscientist's guide to lipidomics. Nat Rev Neurosci 8:743–754. https://doi.org/10.1038/nrn2233
39. Provasek VE, Mitra J, Malojirao VH, Hegde ML (2022) DNA double-strand breaks as pathogenic lesions in neurological disorders. Int J Mol Sci. https://doi.org/10.3390/ijms23094653
40. Rismanchi N, Soderblom C, Stadler J, Zhu PP, Blackstone C (2008) Atlastin GTPases are required for Golgi apparatus and ER morphogenesis. Hum Mol Genet 17:1591–1604. https://doi.org/10.1093/hmg/ddn046
41. Rowe RG, Daley GQ (2019) Induced pluripotent stem cells in disease modelling and drug discovery. Nat Rev Genet 20:377–388. https://doi.org/10.1038/s41576-019-0100-z
42. Salinas S, Proukakis C, Crosby A, Warner TT (2008) Hereditary spastic paraplegia: clinical features and pathogenetic mechanisms. Lancet Neurol 7:1127–1138. https://doi.org/10.1016/S1474-4422(08)70258-8
43. Shribman S, Reid E, Crosby AH, Houlden H, Warner TT (2019) Hereditary spastic paraplegia: from diagnosis to emerging therapeutic approaches. Lancet Neurol 18:1136–1146. https://doi.org/10.1016/S1474-4422(19)30235-2
44. Slabicki M, Theis M, Krastev DB, Samsonov S, Mundwiller E, Junqueira M, Paszkowski-Rogacz M, Teyra J, Heninger AK, Poser I et al (2010) A genome-scale DNA repair RNAi screen identifies SPG48 as a novel gene associated with hereditary spastic paraplegia. PLoS Biol 8:e1000408. https://doi.org/10.1371/journal.pbio.1000408
45. Soliman MA, Aboharb F, Zeltner N, Studer L (2017) Pluripotent stem cells in neuropsychiatric disorders. Mol Psychiatry 22:1241–1249. https://doi.org/10.1038/mp.2017.40
46. Sonda S, Pendin D, Daga A (2021) ER morphology in the pathogenesis of hereditary spastic paraplegia. Cells 10:2870. https://doi.org/10.3390/cells10112870
47. Takahashi K, Tanabe K, Ohnuki M, Narita M, Ichisaka T, Tomoda K, Yamanaka S (2007) Induction of pluripotent stem cells from adult human fibroblasts by defined factors. Cell 131:861–872. https://doi.org/10.1016/j.cell.2007.11.019
48. Thiele C, Hannah MJ, Fahrenholz F, Huttner WB (2000) Cholesterol binds to synaptophysin and is required for biogenesis of synaptic vesicles. Nat Cell Biol 2:42–49. https://doi.org/10.1038/71366
49. Villa GR, Hulce JJ, Zanca C, Bi J, Ikegami S, Cahill GL, Gu Y, Lum KM, Masui K, Yang H et al (2016) An LXR-cholesterol axis creates a metabolic co-dependency for brain cancers. Cancer Cell 30:683–693. https://doi.org/10.1016/j.ccell.2016.09.008

50. Wojcik P, Zarkovic N, Gegotek A, Skrzydlewska E (2020) Involvement of metabolic lipid mediators in the regulation of apoptosis. Biomolecules 10:402. https://doi.org/10.3390/biom10030402
51. Yu J, Vodyanik MA, Smuga-Otto K, Antosiewicz-Bourget J, Frane JL, Tian S, Nie J, Jonsdottir GA, Ruotti V, Stewart R et al (2007) Induced pluripotent stem cell lines derived from human somatic cells. Science 318:1917–1920. https://doi.org/10.1126/science.1151526
52. Zeng H, Guo M, Martins-Taylor K, Wang XF, Zhang Z, Park JW, Zhan SN, Kronenberg MS, Lichtler A, Liu HX et al (2010) Specification of region-specific neurons including forebrain glutamatergic neurons from human induced pluripotent stem cells. PLoS ONE 5:e11853. https://doi.org/10.1371/journal.pone.0011853
53. Zhao XY, Bhattacharyya A (2018) Human models are needed for studying human neurodevelopmental disorders. Am J Hum Genet 103:829–857. https://doi.org/10.1016/j.ajhg.2018.10.009
54. Zhou Y, Zhou B, Pache L, Chang M, Khodabakhshi AH, Tanaseichuk O, Benner C, Chanda SK (2019) Metascape provides a biologist-oriented resource for the analysis of systems-level datasets. Nat Commun 10:1523. https://doi.org/10.1038/s41467-019-09234-6
55. Zhu PP, Denton KR, Pierson TM, Li XJ, Blackstone C (2014) Pharmacologic rescue of axon growth defects in a human iPSC model of hereditary spastic paraplegia SPG3A. Hum Mol Genet 23:5638–5648. https://doi.org/10.1093/hmg/ddu280
56. Zhu PP, Patterson A, Lavoie B, Stadler J, Shoeb M, Patel R, Blackstone C (2003) Cellular localization, oligomerization, and membrane association of the hereditary spastic paraplegia 3A (SPG3A) protein atlastin. J Biol Chem 278:49063–49071. https://doi.org/10.1074/jbc.M306702200
57. Zhu PP, Soderblom C, Tao-Cheng JH, Stadler J, Blackstone C (2006) SPG3A protein atlastin-1 is enriched in growth cones and promotes axon elongation during neuronal development. Hum Mol Genet 15:1343–1353. https://doi.org/10.1093/hmg/ddl054

Publisher's Note